Dalton Transactions

ROYAL SOCIETY OF CHEMISTRY

PAPER

View Article Online
View Journal | View Issue

Cite this: *Dalton Trans.*, 2024, **53**, 4139

Morphology-controlled synthesis of novel nanostructured $Li_4P_2O_7$ with enhanced Li-ion conductivity for all-solid-state battery applications†

Hany El-Shinawi, *[a,b] Edmund J. Cussen [b] and Serena A. Cussen [b]

Mechanical stiffness of oxide-type solid-electrolytes is a major drawback which has hindered their practical application in all-solid-state Li-ion batteries to date. Despite their enhanced structural and electrochemical stabilities, lack of deformability of fast-ion conducting oxides impedes the integration of these materials in bulk-type solid-state cells. Deformable solid-electrolytes such as sulfides, on the other hand, lack sufficient electrochemical stability in contact with conventional cathodes. This has recently triggered a search for new materials that combine high ion-conductivity, deformability and sufficient electrochemical stability. Here, we report the synthesis of a novel form of $Li_4P_2O_7$ that can be densified by cold-pressing and possesses an ion conductivity that is two orders of magnitude higher than conventional $Li_4P_2O_7$ phases. The material is synthesized by a combination of microwave synthesis and chemical lithiation and adopts a nanostructured morphology with a small amorphous component. The material is electrochemically stable at voltages >5 V *vs.* Li^+/Li, which suggests safe use with high-voltage cathodes. The newly-synthesized material is therefore a bulk, deformable analogue of LiPON, with comparable ion conductivity and phase stability. This research highlights the potential of using novel low-temperature synthetic routes to control the morphology and enhance the electrochemical performance of conventional functional materials.

Received 28th December 2023,
Accepted 1st February 2024

DOI: 10.1039/d3dt04377k

rsc.li/dalton

Introduction

Sulfide-type solid electrolytes such as $Li_7P_3S_{11}$ and $Li_{10}GeP_2S_{12}$ are deformable superionic conductors[1,2] which can readily form dense fast-ion conducting electrolyte-layers by cold/warm pressing. These materials, however, have limited electrochemical stability when in contact with conventional cathodes, which is a major drawback that limits their application in bulk-type all-solid-state batteries. Oxide-type solid electrolytes, on the other hand, are more compatible with high-voltage cathodes due to their better electrochemical stability window,[3,4] but, unfortunately, lack deformability that allows the build-up of bulk-type solid-state cells. The search for new solid-electrolytes that possess good ion-conductivity, deformability, and an appropriately wide electrochemical stability window, is underway and has recently been extended to explore new classes of materials such as halide-type solid electrolytes.[5] For oxide-based solid-electrolytes (*e.g.*, garnets and LISICONs), sintering at elevated temperatures is crucial to deliver crystalline phases with sufficient ion-conductivity. This, however, leads to stiff, brittle materials which are difficult to integrate in bulk-type all-solid-state batteries. Recently, we have employed low-temperature synthetic techniques such as microwave synthesis to develop materials with controlled morphology and electrochemical properties.[6–8] Here, we describe our approach to achieve a deformable, nanostructured $Li_4P_2O_7$ phase with promising electrochemical properties.

$Li_4P_2O_7$ is conventionally prepared by solid-state reactions at 700–800 °C (ref. 9 and 10) or by hydrothermal methods (often as multiple-phase mixtures).[11,12] $Li_4P_2O_7$ prepared by solid-state reactions adopts a triclinic symmetry[9,10,13,14] and can be described in terms of P_2O_7 units, built up of two PO_4 tetrahedra sharing vertex, and LiO_4 units. LiO_4 tetrahedra share common edges or vertices, forming a continuous framework containing large voids that are typically available for Li-ion transport. The ionic conductivity of the triclinic $Li_4P_2O_7$ polymorph is reported only at elevated temperatures (*e.g.* 5.6×10^{-3} S cm^{-1} at 450 °C (ref. 10)), suggesting minimal conductivity at ambient conditions. This triclinic polymorph trans-

[a]*Department of Chemistry, Mansoura University, Mansoura, 35516, Egypt. E-mail: h_elshinawi@mans.edu.eg*
[b]*Department of Materials Science and Engineering, University of Sheffield, Sir Robert Hadfield Building, Sheffield, S1 3JD, UK*

† Electronic supplementary information (ESI) available. See DOI: https://doi.org/10.1039/d3dt04377k

forms to a high-temperature monoclinic phase at ~640 °C.[10,15] The formation of the high-temperature phase is accompanied by an increase in the conductivity by approximately a factor of three.[10] It has been suggested that the structural modifications within the monoclinic symmetry lead to a step-wise increase in the rate-limiting apertures that permit passage of Li^+ through the material.[10] Other thermodynamic metastable structural modifications of $Li_4P_2O_7$ are also known in the literature, including a high-pressure monoclinic phase,[11] pseudo-monoclinic (triclinic) phases[12,16] and a trigonal phase.[16] However, these phases are often obtained as multiphase mixtures and have not been isolated in bulk form. In this report, we have employed a combination of microwave synthesis and chemical lithiation to obtain a novel form of $Li_4P_2O_7$ at temperature as low as 400 °C. In addition to an enhanced electrochemical stability window, this phase can be densified by cold-pressing, possessing ion conductivity that is two orders of magnitude higher than that of conventional $Li_4P_2O_7$ phases.

Experimental section

Synthesis

$LiPO_3$ was initially synthesized by a microwave approach.[6] Phosphorus pentasulfide (P_2S_5) and lithium *tert*-butoxide were used as the starting materials. Stoichiometric amounts of the materials were dissolved in tetraglyme at ~130 °C till a clear solution was obtained. 5 ml of this solution (~1 mM) was then heated in a sealed microwave tube for 20 min at 200 °C using a CEM Discover SP microwave synthesizer (2.45 GHz). The resulting product was washed thoroughly with THF (3 × 3 ml) and finally dried in air at 150 °C for 2 h. For chemical lithiation, $LiPO_3$ was mixed with *n*-butyllithium (2.5 M solution in hexane; Sigma Aldrich) in 1 : 2 molar ratio, and stirred overnight under an argon atmosphere. The resulting product was washed thoroughly with hexane (3 × 3 ml) and finally dried in air at 100 °C for 2 h, followed by calcination in air at 400 °C for 4 h.

Characterization

X-ray diffraction (XRD) studies were performed using a PANalytical X'Pert PRO diffractometer in reflection mode using Cu-Kα radiation. *In situ* X-ray diffraction studies were performed using an Anton Paar HTK 1200N heating stage where the samples were heated in the temperature range 25–800 °C under an argon atmosphere. Prior to each XRD measurement, the samples were equilibrated for 1 h at constant temperature followed by 1 h scan at each temperature. A heating rate of 5 °C min^{-1} was employed, and samples were allowed to cool down naturally. Rietveld analyses of diffraction data (12 h scans at room temperature) were performed using the GSAS and EXPGUI programmes, employing a pseudo-Voigt profile function. ICP-MS analysis was performed using an Agilent 7700 ICP-MS instrument. SEM studies were performed using a Zeiss Sigma field emission scanning electron microscope. TEM images were obtained using an FEI Tecnai T20 machine operating at 200 kV. AC impedance and DC polarization measurements were conducted in Swagelok cells assembled under argon atmosphere, and the data were recorded using a Biologic VMP-300 potentiostat. AC impedance data were recorded in the frequency range of 1 MHz to 1 Hz (an electrical perturbation of 50 mV) using gold or lithium electrodes. Gold electrodes were gas-phase deposited on the circular sides of the pellets by thermal evaporation. Prior to each impedance measurement, the samples were equilibrated for 1 h at constant temperature. DC polarization measurements (gold electrodes) were performed by applying voltages in the range of 0.5–1.7 V (8 hours each) and recording the corresponding DC current. To prepare lithium symmetric cells, pellets were sandwiched between two Li foils, and assembled within a Swagelok cell in an Ar-filled glovebox. The surfaces of the used lithium foils were scratched using a stainless-steel blade to obtain clean surfaces before use. The constant current galvanostatic cycling of the symmetric cell was performed using a BioLogic VMP-300 potentiostat by applying a constant current for 2 h, followed by a 10 min OCV before switching to the opposing current direction. For reactivity tests using asymmetric solid-state cells, $Li_4P_2O_7$-C and Li_3PS_4-C composites were initially prepared by mixing either $Li_4P_2O_7$ or Li_3PS_4 with carbon black (10 wt%; KETJENBACK EC-600JD, AkzoNobel) using a pestle and mortar. Three-layer pellets of In/Li_3PS_4/$Li_4P_2O_7$-C and In/Li_3PS_4/Li_3PS_4-C were prepared by pressing In foil (Sigma Aldrich), 60 mg of Li_3PS_4, and 3 mg $Li_4P_2O_7$-C (or Li_3PS_4-C) at 2 tons for 30 s. Indium foil was thinned to ~0.3 mm before use. Thin Cu-foil and Al-foil discs were used to support and collect the current from the anode and the cathode, respectively. Cyclic voltammetry (CV) tests on the assembled cells were performed in Swagelok cells using a BioLogic VMP-300 potentiostat at a scan rate of 0.1 mV s^{-1} in the voltage range 0–5 V *vs.* In/InLi. For reactivity tests using liquid-electrolyte-based cells, electrodes were prepared by mixing $Li_4P_2O_7$ (or ZrO_2) with carbon black and PTFE in the ratio 70 : 20 : 10 wt% using a pestle and mortar, followed by pressing the mixture to form thin pellets. Charge/discharge tests were performed in Swagelok cell using 1 M $LiPF_6$ in EC/DMC (1 : 1) as electrolyte and lithium foil as counter and reference electrodes. Cells containing 3 mg of $Li_4P_2O_7$(ZrO_2)/C/PTFE composites were cycled in the voltage range 1.0–4.5 V at 10 mA g^{-1} current density.

Results and discussion

Microwave-synthesized $LiPO_3$ was used as a precursor to synthesize $Li_4P_2O_7$ through chemical lithiation followed by calcination in air at 400 °C. The material resulted from this process is referred to as $Li_4P_2O_7$-400. Parent $LiPO_3$ was fully characterized in our previous report.[6] Fig. 1 shows how the morphology of as-synthesized $LiPO_3$ is changed by chemical lithiation and the calcination processes to form $Li_4P_2O_7$-400. The porosity is largely retained throughout the stages of the formation of $Li_4P_2O_7$-400, while a significant decrease in the angularity of the particles is observed in the final product. This suggests

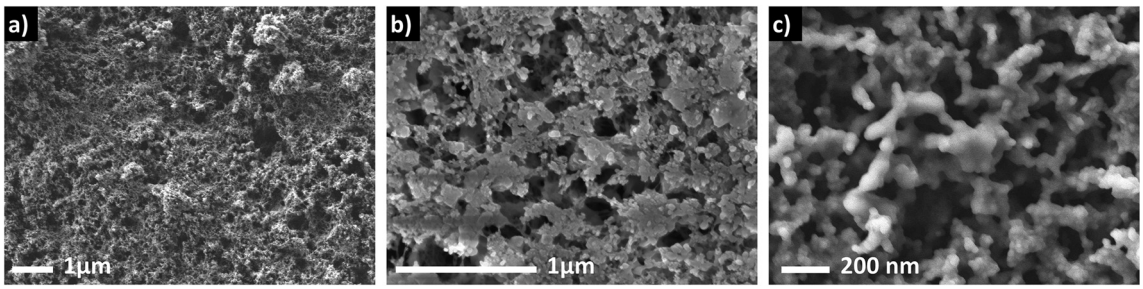

Fig. 1 Morphology evolution of $LiPO_3$ upon chemical lithiation and subsequent calcination. (a) As-synthesized $LiPO_3$; (b) the material after chemical lithiation; (c) the material after lithiation and calcination at 400 °C.

that the heating step facilitates mass transport that permits formation of particles of similar size but with smoother, less anisotropic shapes than the parent $LiPO_3$. Sintering at temperatures higher than 400 °C was avoided to maintain the nanostructured morphology (and deformability) of the material. $Li_4P_2O_7$-400 showed a large specific surface area of 31.1 $m^2 g^{-1}$, as determined from nitrogen adsorption using the Brunauer–Emmett–Teller (BET) method. Elemental analysis by ICP-MS revealed a Li : P molar ratio of 2.06(1) : 1, indicating the conversion of $LiPO_3$ to $Li_4P_2O_7$.

XRD data collected from $Li_4P_2O_7$-400 are shown in Fig. 2. Data collected from the as-made material show significant broadened peaks at similar *d*-spacings to those anticipated for the low-temperature triclinic form of $Li_4P_2O_7$ (Fig. 2b). In order to evaluate the structure of $Li_4P_2O_7$-400, additional diffraction patterns were collected *in situ* as this material was heated to 800 °C and subsequently cooled to room temperature (Fig. 2a). These data show a largely invariant diffraction pattern as the sample is heated from room temperature to 500 °C, but, between 500 and 600 °C the Bragg peaks sharpen and this permits resolution of multiple peaks that were extensively overlapped in the as-made material. Heating further to 700 °C shows a simplification of the pattern with fewer peaks being observed. Heating to 800 °C causes further sharpening of the peaks and enables comparison of the structure with the monoclinic phase previously observed for $Li_4P_2O_7$ above *ca.* 640 °C.[10] On cooling this sample from 800 °C to room temperature, a diffraction pattern characteristic of conventional low-temperature $Li_4P_2O_7$ phase, with no traces of impurities, is obtained (see Fig. S1† for XRD refinement). A second cycle of heating/cooling (Fig. S2†) shows the anticipated conversion of the low-temperature $Li_4P_2O_7$ phase to the high-temperature modification,[10,15] with no appearance of the $Li_4P_2O_7$-400 phase. The appearance of the established triclinic to monoclinic phase transition in subsequent heating cycles indicates that $Li_4P_2O_7$-400 is a form of $Li_4P_2O_7$ that likely lacks full crystallinity. The X-ray diffraction data collected from $Li_4P_2O_7$-400 were readily indexed in a monoclinic crystal system, with unit

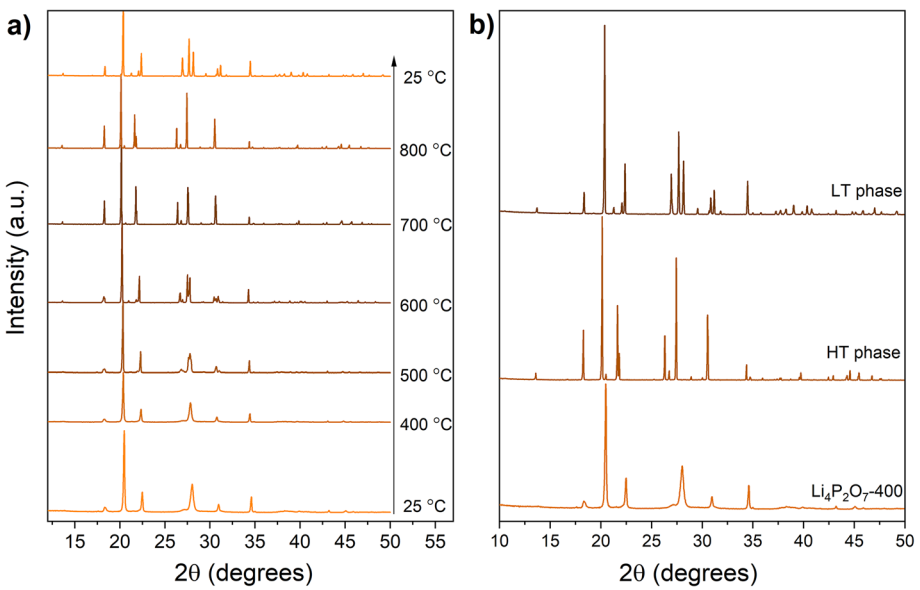

Fig. 2 (a) *In situ* XRD analysis of $Li_4P_2O_7$-400 through heating from room temperature to 800 °C, then cooling back to room temperature. (b) A highlight of the XRD patterns of $Li_4P_2O_7$-400, high-temperature (HT) $Li_4P_2O_7$ phase and the conventional low-temperature (LT) $Li_4P_2O_7$ phase.

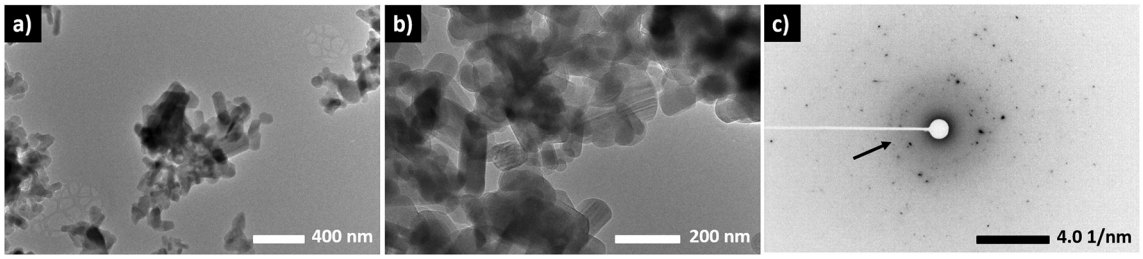

Fig. 3 TEM images (a and b) and SAED pattern (c) collected from a $Li_4P_2O_7$-400. Diffuse rings, which indicate a small degree of amorphousness, are arrowed.

cell parameters related to the high-temperature phase (with an appropriate consideration of the effects of lattice expansion due to temperature elevation). Rietveld structural refinement against the diffraction data were performed employing the structure model of the high-temperature phase,[10] resulting in refined unit cell parameters of a = 8.6181(6), b = 5.1863(2), c = 13.1373(1) Å, and β = 103.624(5)°. The refined XRD data are depicted in Fig. 4, and the refinement parameters are summarized in Table S1.† The fact that the material displays considerable peak broadening leading to a larger degree of peak overlap, together with the limited accuracy of X-rays to locate light elements such as lithium and oxygen, however, limits the precision of the crystal structure analysis when compared to the refinement against the high temperature dataset shown in Fig. S1.†

TEM analysis of $Li_4P_2O_7$-400 indicates a good crystallinity of the material with a small contribution from an amorphous phase. Fig. 3 shows TEM images collected from selected parts of the sample. It is worth mentioning here that the samples were highly sensitive to the beam which prevented higher-magnification imaging. The sample contained rod-shaped particles of ~200–400 nm length and smaller interconnected particles with undefined shape. The rod-shaped particles had sharp edges with no visible amorphous coating. The particles overlap showing a striped appearance in some parts which may be Moire fringes. Diffraction patterns collected from different areas of the sample showed irregular spot patterns indicative of single crystal ordering (Fig. 3c). The irregular appearance is due to imaging multiple particles together. In addition to the spot patterns, there is a weak diffuse ring pattern, which differs greatly from the diffraction pattern of the support material, suggesting a degree of amorphousness. A small contribution from an amorphous phase is attributed to the low synthesis temperature, and helps to preserve the deformability of the material as discussed below.

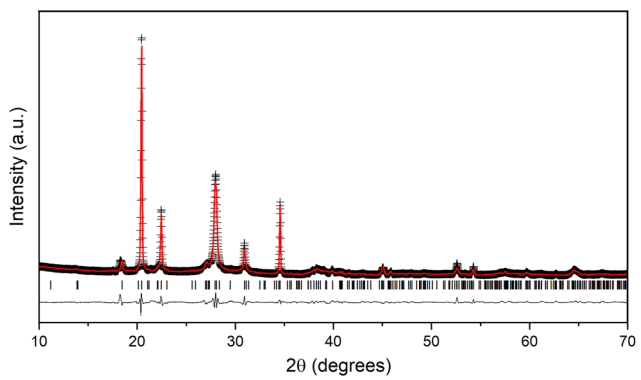

Fig. 4 Observed (+), calculated (red) and difference (black) patterns of the Retiveld analysis of the XRD data collected from $Li_4P_2O_7$-400 at room temperature.

The structural characterisation, hence, shows that $Li_4P_2O_7$-400 represents a new modification of monoclinic $Li_4P_2O_7$ in a nanostructured morphology with a small contribution of an amorphous phase. This novel morphology has, interestingly, allowed the densification of the material by cold-pressing. Pellets of $Li_4P_2O_7$-400 cold-pressed at 250 MPa achieved a density that is approximately 84% of the theoretical density. These cold-pressed pellets were used to study ion and electron conductivities of the material using impedance spectroscopy and DC polarization measurements. For comparison, a sample of $Li_4P_2O_7$ heated at 800 °C was examined by impedance spectroscopy to offer conductivity data for the conventional low-temperature $Li_4P_2O_7$ phase ($Li_4P_2O_7$-800). $Li_4P_2O_7$-800 was an extremely poor conductor at room temperature, showing an undetectably small current in the impedance measurements. Raising the temperature to 80 °C, allowed an estimation of the conductivity as 2.7×10^{-8} S cm^{-1}. A cold-pressed sample of $Li_4P_2O_7$-400, on the other hand, showed a conductivity of 1.2×10^{-6} S cm^{-1} at the same temperature. The two orders of magnitude increase in conductivity is evident in the comparison of the impedance plots of $Li_4P_2O_7$-400 and conventional $Li_4P_2O_7$ ($Li_4P_2O_7$-800) shown in Fig. 5. The impedance of $Li_4P_2O_7$-400 is composed of a single semicircle and a low-frequency linear increase in impedance. The latter observation typically arises from blocking of Li^+ conduction at the gold electrodes and suggests that the observed transport effect is mainly ionic and corresponds to Li-ion mobility. The data were successfully fitted using a conventional equivalent circuit that employs a constant phase element (Q) in parallel to a resistance element (R) to represent the semicircle ([RQ]), and a constant phase element to represent the low frequency spike ([Q]). The capacitance (C) calculated from the fit parameter Q of the high-frequency semicircle is $\sim 8 \times 10^{-11}$ F. This value accounts well for a combination of bulk and grain-boundary resistances.[17,18]

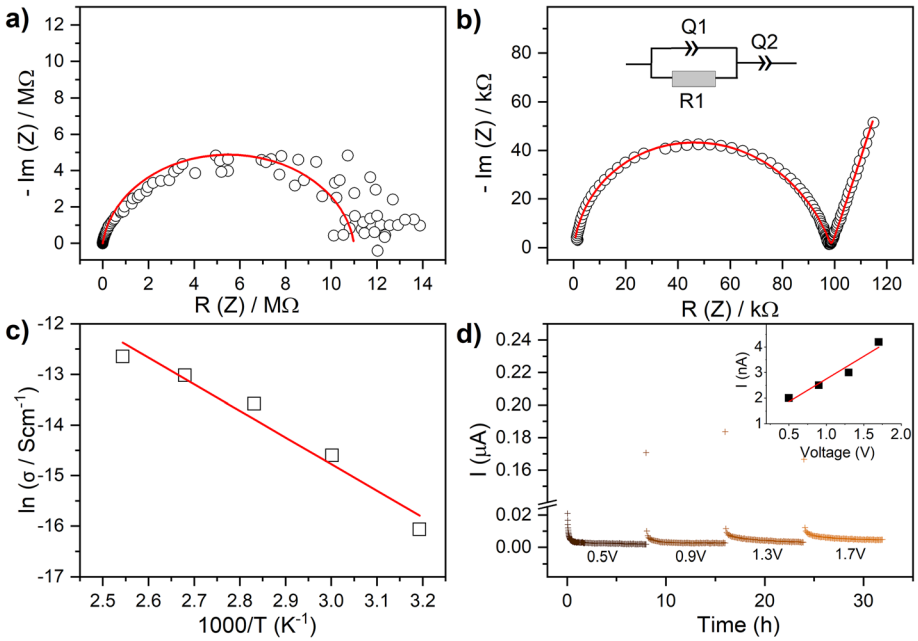

Fig. 5 (a) Impedance collected from low-temperature $Li_4P_2O_7$ phase ($Li_4P_2O_7$-800) at 80 °C. (b) Impedance collected from $Li_4P_2O_7$-400 at 80 °C. (c) The Arrhenius plot of the conductivity data of $Li_4P_2O_7$-400 collected in the temperature range 40–120 °C. (d) DC polarization tests and corresponding *I*/*V* curve (inset) for $Li_4P_2O_7$-400 at 80 °C.

Hence, similar to deformable sulfide-type solid-electrolytes, $Li_4P_2O_7$-400 impedance showed a single semicircle representing bulk and grain-boundary resistances as an indication of a good sinterability achieved *via* cold pressing. The activation energy (E_a) for the total conductivity of the material in the temperature range 40–120 °C is obtained from the Arrhenius plot of $\sigma = \sigma_0 \exp(-E_a/kT)$, where σ_0 is the pre-exponential factor, k is the Boltzmann constant, T is the absolute temperature. The Arrhenius plot is shown in Fig. 5c, revealing an activation of 0.45(1) eV. In order to investigate the electronic contribution to the measured conductivity of $Li_4P_2O_7$-400, DC polarization tests were employed to estimate the electronic conductivity of the material by applying voltages in the range 0.7–1.5 V (Fig. 5d). These tests revealed an electronic conductivity of $1.8(3) \times 10^{-9}$ S cm^{-1} at 80 °C, which clearly suggests that the observed conductivity of $Li_4P_2O_7$-400 (1.2×10^{-6} S cm^{-1} at 80 °C) is almost entirely ionic.

The newly-synthesized $Li_4P_2O_7$, hence, possesses an enhanced ion conductivity compared with conventional $Li_4P_2O_7$ and γ-Li_3PO_4 (<10^{-12} S cm^{-1} at 100 °C (ref. 19)) phases. The improved conductivity can be attributed to the modified structure and morphology of the material. The modified morphology, including the nanostructured nature and a small contribution from an amorphous material, allowed good contact between the grains by simple cold-pressing which reduces of the grain-boundary resistance. The modified crystal structure also seems to favour an improved ion transport in the material. A monoclinic modification of the material is reported to trigger an enhanced Li-ion transport in the material through migration channels with extended cross-sections.[10,12] The conductivity of the new $Li_4P_2O_7$ form (1.2×10^{-6} S cm^{-1} at 80 °C) remains too low to run a full solid-state cell at room temperature. However, considering the enhanced electrochemical stability of the material (see below), the new material clearly would have remarkable properties compared with other materials which fall into the same category. The conductivity of the new $Li_4P_2O_7$ at 80 °C is comparable to that of LiPON films at room temperature (~10^{-6} S cm^{-1} (ref. 20 and 21)), and that of recently-reported bulk $Li_{3.6}PO_{3.4}N_{0.6}$ (5.0×10^{-6} S cm^{-1} at 70 °C (ref. 22)) and well above that of other bulk phosphorus oxynitrides such as $Li_{0.88}PO_{3.73}N_{0.14}$ (1.4×10^{-13} S cm^{-1} at RT[23]) and Li_2PO_2N (8.8×10^{-7} S cm^{-1} at 80 °C (ref. 24)). None of the above materials, nevertheless, is densified by cold-pressing, which makes the new $Li_4P_2O_7$ phase more suitable for application in bulk-type all-solid-sate cells that operate at intermediate temperatures.

To study the possible use of $Li_4P_2O_7$-400 in contact with high-voltage electrodes, the electronic stability window of the material was checked by cyclic voltammetry (CV) in the voltage range 0–5 V *vs.* In/InLi. An asymmetric In/Li_3PS_4/$Li_4P_2O_7$-C cell was used to collect the CV data. In this cell, Li_3PS_4 is used as the solid-electrolyte because it has an enhanced ion conductivity compared with $Li_4P_2O_7$, which provides a reliable performance of the cell. $Li_4P_2O_7$ intimately mixed with carbon black (10 wt%) was used as the working electrode. The cyclic voltammetry of this cell is compared with the performance of an identical cell containing Li_3PS_4/C as the active material (In/Li_3PS_4/Li_3PS_4-C) in Fig. 6a. Unlike Li_3PS_4, $Li_4P_2O_7$ possess remarkable stability, showing no evidence of electrochemical reactivity up to 5 V *vs.* In/InLi (~5.6 V *vs.* Li^+/Li). The absence

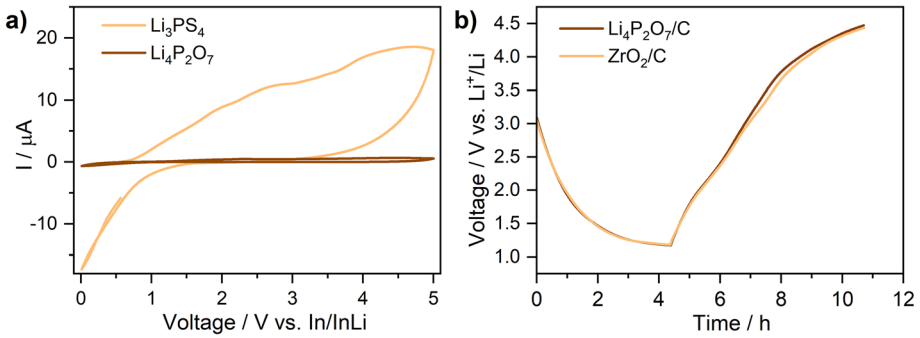

Fig. 6 (a) CV data collected from the asymmetric (solid-state) cells In/Li_3PS_4/$Li_4P_2O_7$-C and In/Li_3PS_4/Li_3PS_4-C at room temperature with a scan rate of 0.1 mV s^{-1}. (b) Discharge–charge curves of two liquid-electrolyte-based half cells employing $Li_4P_2O_7$/C or ZrO_2/C as the working electrode and Li metal as counter electrode (current density = 10 mA g^{-1}).

of any significant phase decomposition in this voltage range, compared with standard Li_3PS_4, suggests that the material is suitable for high-voltage applications. In order to further confirm the electrochemical stability of $Li_4P_2O_7$-400 at high voltages, a cell employing a liquid electrolyte and $Li_4P_2O_7$/C as an active material (Li/liquid-electrolyte/$Li_4P_2O_7$-C), was cycled at a low current density (10 mA g^{-1}) in the voltage range 1–4.5 V (*vs.* Li^+/Li). Higher voltages were avoided to avoid a series decomposition of the liquid electrolyte. The cell was compared with an identical standard cell containing inert ZrO_2/C as the active material. The two cells showed identical charge/discharge curves under same experimental conditions, confirming the stability of $Li_4P_2O_7$ (Fig. 6b).

In order to examine the compatibility of $Li_4P_2O_7$-400 with Li metal anodes, a symmetric Li/$Li_4P_2O_7$/Li cell was studied. A notable increase of the impedance of the cell, compared with Au/$Li_4P_2O_7$/Au cells, was observed which suggests a resistive interface between Li metal and $Li_4P_2O_7$. The area specific resistance (ASR) for the Li/$Li_4P_2O_7$ interface is estimated to be greater than the resistance of the pellet by a factor of three (Fig. S3†). Similar behaviour was observed for related phosphate-based solid-electrolytes such as $LiZr_2(PO_4)_3$.[25] The observed high interfacial resistance may be partially related to an insufficient contact between Li metal and the pellet, but also clearly indicates instability of $Li_4P_2O_7$ in contact with Li.

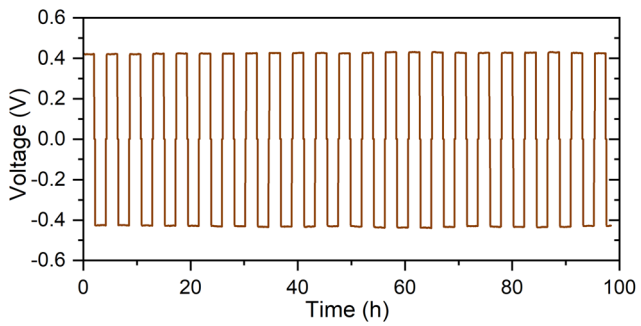

Fig. 7 Galvanostatic cycling data of a Li/$Li_4P_2O_7$/Li symmetric cell at 80 °C and 2 μA cm^{-2} current density.

This could also be visually observed as a darkening of the pellet's surface after contact with Li. This is consistent with the electrochemical stability data of related phosphates, including $LiZr_2(PO_4)_3$ [25] and LiPON,[26] which revealed the formation of a passivation layer at the surface of the solid-electrolyte in contact with Li metal. The stability of the Li/$Li_4P_2O_7$ interface upon lithium dissolution/deposition was tested by cycling a symmetric Li/$Li_4P_2O_7$/Li at current density of 2 μA cm^{-2} at 80 °C (Fig. 7). A low current density was employed to compensate for the high resistance of the material (see ref. 22). A very stable cycle performance, with insignificant increase of the cell voltage upon cycling for 100 h, is observed which indicates a good stability of the interface. This result is consistent with the behaviour of related phosphate-based solid-electrolytes such as $LiZr_2(PO_4)_3$,[26] LiPON[26] and bulk $Li_{3.6}PO_{3.4}N_{0.6}$,[22] which are believed to form stable interfaces with Li metal.

Conclusions

A nanostructured form of $Li_4P_2O_7$ has been successfully synthesized by chemical lithiation of microwave-synthesized $LiPO_3$ followed by calcination at 400 °C. The new $Li_4P_2O_7$ form preserves the nanostructured morphology of parent $LiPO_3$, and exhibits a monoclinic structure which is related to the high-temperature $Li_4P_2O_7$ phase. The novel morphology of the material, including a nanostructured nature and a small contribution from an amorphous phase, allowed the densification of the material by cold-pressing, exhibiting an ion conductivity that is approximately two orders of magnitude higher than that of $Li_4P_2O_7$ formed by conventional syntheses. This improved conductivity is attributed to both the modified morphology and the modified crystal structure of the material. The material also showed no evidence of electrochemical decomposition at voltages up to 5.6 V *vs.* Li^+/Li, which suggests possible use in contact with high-voltage cathodes. In contact with Li metal, $Li_4P_2O_7$ forms a resistive interface, which was found to be very stable upon Li^+ dissolution/deposition. The newly-synthesized $Li_4P_2O_7$, hence, possesses ion conductivity and phase

stability comparable to LiPON phases, but eventually can be prepared in a bulk, deformable form.

Conflicts of interest

There are no conflicts of interest to declare.

Acknowledgements

This work was supported by the ICSF Faraday Challenge project SOLBAT, UK [grant FIRG007], and the Academy of Scientific Research and Technology, Egypt [grant RESPECT-10025].

References

1 N. Kamaya, K. Homma, Y. Yamakawa, M. Hirayama, R. Kanno, M. Yonemura, T. Kamiyama, Y. Kato, S. Hama, K. Kawamoto and A. Mitsui, A lithium superionic conductor, *Nat. Mater.*, 2011, **10**, 682–686, DOI: 10.1038/nmat3066.

2 Y. Seino, T. Ota, K. Takada, A. Hayashi and M. Tatsumisago, A sulphide lithium super ion conductor is superior to liquid ion conductors for use in rechargeable batteries, *Energy Environ. Sci.*, 2014, **7**, 627–631, DOI: 10.1039/C3EE41655K.

3 T. Thompson, S. Yu, L. Williams, R. D. Schmidt, R. Garcia-Mendez, J. Wolfenstine, J. L. Allen, E. Kioupakis, D. J. Siegel and J. Sakamoto, Electrochemical Window of the Li-Ion Solid Electrolyte Li7La3Zr2O12, *ACS Energy Lett.*, 2017, **2**(2), 462–468, DOI: 10.1021/acsenergylett.6b00593.

4 Y. Zhu, X. He and Y. Mo, Origin of Outstanding Stability in the Lithium Solid Electrolyte Materials: Insights from Thermodynamic Analyses Based on First-Principles Calculations, *ACS Appl. Mater. Interfaces*, 2015, **7**, 23685–23693, DOI: 10.1021/acsami.5b07517.

5 C. Wang, J. Liang, J. T. Kim and X. Sun, Prospects of halide-based all-solid-state batteries: From material design to practical application, *Sci. Adv.*, 2022, **8**, eadc9516, DOI: 10.1126/sciadv.adc9516.

6 H. El-Shinawi, E. J. Cussen and S. A. Corr, Morphology-Directed Synthesis of LiFePO4 and LiCoPO4 from Nanostructured Li1+2xPO3+x, *Inorg. Chem.*, 2019, **58**(10), 6946.

7 H. El-Shinawi, E. J. Cussen and S. A. Corr, A facile synthetic approach to Nanostructured Li2S cathodes for rechargeable solid-state Li–S batteries, *Nanoscale*, 2019, **11**, 19297.

8 H. El-Shinawi, E. J. Cussen and S. A. Corr, Selective and Facile Synthesis of Sodium Sulfide and Sodium Disulfide Polymorphs, *Inorg. Chem.*, 2018, **57**(13), 7499.

9 A. Daidouh, M. L. Veiga, C. Pico and M. Martinez-Ripoll, A New Polymorph of Li4P2O7, *Acta Crystallogr., Sect. C: Cryst. Struct. Commun.*, 1997, **53**, 167, DOI: 10.1107/S0108270196011869.

10 V. I. Voronin, E. A. Sherstobitova, V. A. Blatov and G. S. Shekhtman, Lithium-cation conductivity and crystal structure of lithium diphosphate, *J. Solid State Chem.*, 2014, **211**, 170.

11 O. V. Yakubovich and O. K. Mel'nikov, Crystal Structure of the Li4P2O7 Compound, *Crystallogr. Rep.*, 1994, **34**, 737.

12 E. L. Belokoneva, A. A. Gaganina, O. V. Dimitrova and A. S. Volkov, Polymorphism of Li4P2O7: New Modification and Identification of Structural Subfamilies by Topology and Symmetry Analysis, *Crystallogr. Rep.*, 2022, **67**, 348–355, DOI: 10.1134/S1063774522030051.

13 Y. A. Du and N. A. W. Holzwarth, First-principles study of LiPON and related solid electrolytes, *Phys. Rev. B: Condens. Matter Mater. Phys.*, 2010, **81**, 184106.

14 N. A. W. Holzwarth, N. D. Lepley and Y. A. Du, Computer modeling of lithium phosphate and thiophosphate electrolyte materials, *J. Power Sources*, 2011, **196**, 6870–6876, DOI: 10.1016/j.jpowsour.2010.08.042.

15 T. Y. Tien and F. A. Hummel, Studies in Lithium Oxide Systems: Lithium Phosphate Compounds, *J. Am. Ceram. Soc.*, 1961, **44**, 206, DOI: 10.1111/j.1151-2916.1961.tb15361.x.

16 B. Raguž, K. Wittich and R. Glaum, Two New, Metastable Polymorphs of Lithium Pyrophosphate Li4P2O7, *Eur. J. Inorg. Chem.*, 2019, 1688–1696, DOI: 10.1002/ejic.201801100.

17 J. T. S. Irvine, D. C. Sinclair and A. R. West, Electroceramics Characterization by Impedance Spectroscopy, *Adv. Mater.*, 1990, **2**, 132–138.

18 W. B. Reid and A. R. West, Atmospheric attack on lithium silicate glass, *Solid State Ionics*, 1988, **681**, 28–30.

19 S. Muy, J. C. Bachman, H. H. Chang, L. Giordano, F. Maglia, S. Lupart, P. Lamp, W. G. Zeier and Y. Shao-Horn, Lithium conductivity and Meyer-Neldel rule in Li3PO4-Li3VO4-Li4GeO4 lithium superionic conductors, *Chem. Mater.*, 2018, **30**(16), 5573–5582, DOI: 10.1021/acs.chemmater.8b01504.

20 X. Yu, J. B. Bates, G. E. Jellison and F. X. Hart, A Stable Thin-Film Lithium Electrolyte: Lithium Phosphorus Oxynitride, *J. Electrochem. Soc.*, 1997, **144**(2), 524–532, DOI: 10.1149/1.1837443.

21 J. B. Bates, N. J. Dudney, G. R. Gruzalski, R. A. Zuhr, A. Choudhury, C. F. Luck and J. D. Robertson, Fabrication and Characterization of Amorphous Lithium Electrolyte Thin Films and Rechargeable Thin-Film Batteries, *J. Power Sources*, 1993, **43**(1), 103–110, DOI: 10.1016/0378-7753(93)80106-Y.

22 P. López-Aranguren, M. Reynaud, P. Głuchowski, A. Bustinza, M. Galceran, J. M. López-del-Amo, M. Armand and M. Casas-Cabanas, Crystalline LiPON as a Bulk-Type Solid Electrolyte, *ACS Energy Lett.*, 2021, **6**(2), 445–450, DOI: 10.1021/acsenergylett.0c02336.

23 B. Wang, B. C. Chakoumakos, B. C. Sales, B. S. Kwak and J. B. Bates, Synthesis, Crystal Structure, and Ionic Conductivity of a Polycrystalline Lithium Phosphorus

Oxynitride with the γ-Li3PO4 Structure, *J. Solid State Chem.*, 1995, **115**(2), 313–323, DOI: **10.1006/jssc.1995.1140**.

24 K. Senevirathne, C. S. Day, M. D. Gross, A. Lachgar and N. A. W. Holzwarth, A New Crystalline LiPON Electrolyte: Synthesis, Properties, and Electronic Structure, *Solid State Ionics*, 2013, **233**, 95–101, DOI: **10.1016/j.ssi.2012.12.013**.

25 H. El-Shinawi, A. Regoutz, D. J. Payne, E. J. Cussen and S. A. Corr, NASICON LiM2(PO4)3 electrolyte (M=Zr) and electrode (M=Ti) materials for all solid-state Li-ion batteries with high total conductivity and low interfacial resistance, *J. Mater. Chem. A*, 2018, **6**, 5296.

26 D. Cheng, T. A. Wynn, X. Wang, S. Wang, M. Zhang, R. Shimizu, S. Bai, H. Nguyen, C. Fang, M. Kim, W. Li, B. Lu, S. J. Kim and Y. S. Meng, Unveiling the Stable Nature of the Solid Electrolyte Interphase between Lithium Metal and LiPON via Cryogenic Electron Microscopy, *Joule*, 2020, **4**(11), P2484–P2500, DOI: **10.2139/ssrn.3640837**.